


# Dissipative preparation of multipartite Greenberger-Horne-Zeilinger states of Rydberg atoms

Chong Yang(杨崇), Dong-Xiao Li(李冬啸), and Xiao-Qiang Shao(邵晓强)†

**Citation:**Chin. Phys. B, 2021, 30 (**2**): 023201. DOI: 10.1088/1674-1056/abd755
Journal homepage: http://cpb.iphy.ac.cn; http://iopscience.iop.org/cpb

**What follows is a list of articles you may be interested in**

---

## Probing time delay of strong-field resonant above-threshold ionization

Shengliang Xu(徐胜亮), Qingbin Zhang(张庆斌), Cheng Ran(冉成), Xiang Huang(黄湘), Wei Cao(曹伟), and Peixiang Lu(陆培祥)

Chin. Phys. B, 2021, 30 (**1**): 013202. DOI: 10.1088/1674-1056/abc7a5

## Precise measurement of a weak radio frequency electric field using a resonant atomic probe

Liping Hao(郝丽萍), Yongmei Xue(薛咏梅), Jiabei Fan(樊佳蓓), Jingxu Bai(白景旭), Yuechun Jiao(焦月春), Jianming Zhao(赵建明)

Chin. Phys. B, 2020, 29 (**3**): 033201. DOI: 10.1088/1674-1056/ab6c49

## Tunable multistability and nonuniform phases in a dimerized two-dimensional Rydberg lattice

Han-Xiao Zhang(张焓笑), Chu-Hui Fan(范楚辉), Cui-Li Cui(崔淬砺), Jin-Hui Wu(吴金辉)

Chin. Phys. B, 2020, 29 (**1**): 013204. DOI: 10.1088/1674-1056/ab5d06

## Rydberg electromagnetically induced transparency and Autler-Townes splitting in a weak radio-frequency electric field

Liping Hao(郝丽萍), Yongmei Xue(薛咏梅), Jiabei Fan(樊佳蓓), Yuechun Jiao(焦月春), Jianming Zhao(赵建明), Suotang Jia(贾锁堂)

Chin. Phys. B, 2019, 28 (**5**): 053202. DOI: 10.1088/1674-1056/28/5/053202

## Properties of collective Rabi oscillations with two Rydberg atoms

Dan-Dan Ma(马丹丹), Ke-Ye Zhang(张可烨), Jing Qian(钱静)

Chin. Phys. B, 2019, 28 (**1**): 013202. DOI: 10.1088/1674-1056/28/1/013202

---

SPECIAL TOPIC — Quantum computation and quantum simulation

# Dissipative preparation of multipartite Greenberger–Horne–Zeilinger states of Rydberg atoms*

Chong Yang(杨崇)[1,2], Dong-Xiao Li(李冬啸)[3], and Xiao-Qiang Shao(邵晓强)[1,2,†]

[1] Center for Quantum Sciences and School of Physics, Northeast Normal University, Changchun 130024, China
[2] Center for Advanced Optoelectronic Functional Materials Research, and Key Laboratory for UV Light-Emitting Materials and Technology of Ministry of Education, Northeast Normal University, Changchun 130024, China
[3] School of Physics, International Joint Laboratory on Quantum Sensing and Quantum Metrology, Huazhong University of Science and Technology, Wuhan 430074, China

(Received 14 October 2020; revised manuscript received 20 November 2020; accepted manuscript online 30 December 2020)

The multipartite Greenberger–Horne–Zeilinger (GHZ) states play an important role in large-scale quantum information processing. We utilize the polychromatic driving fields and the engineered spontaneous emissions of Rydberg states to dissipatively drive three- and four-partite neutral atom systems into the steady GHZ states, at the presence of the next-nearest neighbor interaction of excited Rydberg states. Furthermore, the introduction of quantum Lyapunov control can help us optimize the dissipative dynamics of the system so as to shorten the convergence time of the target state, improve the robustness against the spontaneous radiations of the excited Rydberg states, and release the limiting condition for the strengths of the polychromatic driving fields. Under the feasible experimental conditions, the fidelities of three- and four-partite GHZ states can be stabilized at 99.24% and 98.76%, respectively.

**Keywords:** multipartite entanglement, Lyapunov control, Rydberg antiblockade, quantum dissipation

**PACS:** 32.80.Ee, 02.30.Yy, 03.65.Ud, 42.50.Lc **DOI:** 10.1088/1674-1056/abd755

## 1. Introduction

Quantum entanglement is one of the most remarkable features in quantum physics, as well as a valuable resource in the fields of quantum communication,[1–6] quantum computing,[7–12] and other quantum information processing.[13–22] With the development of quantum information science, bipartite entanglement has been intensively explored, and several milestones have been achieved.[23–25] In recent years, researchers have become increasingly interested in the study of multipartite entanglements. Compared with bipartite entanglement, multipartite entanglement can better reflect the nonlocality of quantum physics.[26] Greenberger–Horne–Zeilinger (GHZ) states represent a paradigmatic example of genuine multipartite entangled states. Because of the large information capacity, GHZ states have been used extensively in quantum secret sharing,[27–29] quantum teleportation,[30–32] and multipartite nonlocality tests.[33,34] Therefore, the generation and measurement of GHZ states with various systems and methods have become an attractive research field.

Rydberg atoms have been considered as a promising candidate among most applications of quantum information science.[35–41] The strong, long-range dipole–dipole or van der Waals interactions between Rydberg atoms will lead to the so-called Rydberg blockade effect, which suppresses the simultaneous excitation of two or more atoms into the same Rydberg state. Ever since the seminal scheme was proposed by Jaksch and coworkers,[42] a variety of proposals were designed for quantum information processing using the Rydberg blockade, such as quantum algorithms,[43,44] entanglement generation,[45–48] quantum repeaters,[49–51] single-photon transistors.[52] In contrast to the blockade regime, the Rydberg antiblockade, which can achieve the simultaneous excitations of two Rydberg atoms, offers many new possibilities in the research of quantum logic gate[53–63] and quantum entanglement.[64–72] Quite recently, the authors of Ref. [73] provide a powerful approach for simulating quantum cellular automata and generating GHZ states with even numbers of particles restricted to nearest-neighbor interactions based on Rydberg antiblockade. Nevertheless, the next-nearest neighbor interaction of Rydberg atoms cannot be neglected within the parameters they consider, unless the case of three Rydberg atoms arranged in an equilateral triangle.[74]

To compensate for the defects in Refs. [73,74], we now design a more general strategy that can be used to produce GHZ states with both odd and even numbers of particles. This scheme is able to obtain the steady GHZ state in the presence of the next-nearest neighbor interaction by appropriately adjusting the frequency of the driving fields and the relevant detuning. Without loss of generality, we discuss in detail the preparation of GHZ states in three- and four-partite systems. The numerical simulation results show that the population of the target state in our scheme can reach more than 99%. In

*Project supported by the National Natural Science Foundation of China (Grant Nos. 11774047 and 12047525).
†Corresponding author. E-mail: shaoxq644@nenu.edu.cn
© 2021 Chinese Physical Society and IOP Publishing Ltd 

addition, we introduce external coherent control fields to accelerate the dissipative dynamics and widen the range of parameters, where the strength of the control fields is designed by the Lyapunov control theory. It is worth noting that the robustness of the optimized scheme against the spontaneous emissions of Rydberg states has also been greatly enhanced.

## 2. Preparation of tripartite GHZ state

### 2.1. Model

The system includes three identical Rydberg atoms, with each consisting of a ground state $|g\rangle$, a Rydberg state $|r\rangle$, and a temporary (short-lived) level $|e\rangle$. For simplicity, we just take three atoms arranged into an isosceles right triangle as an example (not limited to this specific alignment of atoms). The one at the right angle is atom 2, and the other two are labeled as atom 1 and atom 3. As shown in Fig. 1, the transitions from the ground state $|g\rangle$ to the Rydberg state $|r\rangle$ of atom 1 and atom 3 are driven by the polychromatic fields $\Omega_{1,2,4,5}$ with detunings $-\Delta_{1,2,4,5}$, while the polychromatic fields $\Omega_{1,2,3}$ with detunings $-\Delta_{1,2,3}$ are applied to drive the transition $|g\rangle \leftrightarrow |r\rangle$ of the atom 2. In addition, the resonant coupling between ground state $|g\rangle$ and the short-lived state $|e\rangle$ is realized by the classical laser field of Rabi frequency $\Omega_0$, and the atomic decay rate from the short-lived state $|e\rangle$ to the ground state $|g\rangle$ is $\Gamma$. Then the master equation of the whole system, after neglecting the decay of Rydberg states for the moment, can be expressed by the Lindblad form (assuming $\hbar = 1$)

$$\dot{\rho} = -\mathrm{i}[H,\rho] + \sum_{j=1}^{3} L_j \rho L_j^{\dagger} - \frac{1}{2}(L_j^{\dagger}L_j\rho + \rho L_j^{\dagger}L_j), \tag{1}$$

where the Hamiltonian in the interaction picture can be written as

$$\begin{aligned} H \;=\; & \sum_{j=1}^{3}(\Omega_0\sigma_j^{re} + \Omega_1\sigma_j^{rg}\,\mathrm{e}^{-\mathrm{i}\Delta_1 t} + \Omega_2\sigma_j^{rg}\,\mathrm{e}^{-\mathrm{i}\Delta_2 t}) \\ & + \Omega_3\sigma_2^{rg}\,\mathrm{e}^{-\mathrm{i}\Delta_3 t} + \Omega_4\sigma_1^{rg}\,\mathrm{e}^{-\mathrm{i}\Delta_4 t} + \Omega_4\sigma_3^{rg}\,\mathrm{e}^{-\mathrm{i}\Delta_4 t} \\ & + \Omega_5\sigma_1^{rg}\,\mathrm{e}^{-\mathrm{i}\Delta_5 t} + \Omega_5\sigma_3^{rg}\,\mathrm{e}^{-\mathrm{i}\Delta_5 t} + \sum_{j\neq k} U_{jk}\sigma_j^{rr}\sigma_k^{rr}, \end{aligned} \tag{2}$$

and the Lindblad operators describing the spontaneous decay out of the state $|e\rangle$ are denoted by $L_j = \sqrt{\Gamma}\sigma_j^{ge}$ with atomic operators $\sigma_j^{mn} = |m_j\rangle\langle n_j|$ for atom $j$. In Eq. (2), $U_{jk}$ stands for the Rydberg interaction strength, originated from the long-range van der Waals interaction proportional to $C_6/r_{jk}^6$, where $r_{jk}$ is the distance between the $j$-th and the $k$-th Rydberg atoms and $C_6$ depends on the atomic principal quantum numbers.[75] Since three Rydberg atoms are arranged in an isosceles right triangle, the atomic distance is $r_{12} = r_{23} = r$ and $r_{13} = \sqrt{2}r$. Then the corresponding Rydberg interactions comply with the condition $U_{12} = U_{23} = U$ and $U_{13} = U/8$. Now we reformulate the Hamiltonian in a rotating frame with respect to $U_0 = \exp\left(-\mathrm{i}t\sum_{j\neq k} U_{jk}\sigma_j^{rr}\sigma_k^{rr}\right)$ and obtain

$$H_{\mathrm{I}} = H_g + H_e, \tag{3}$$

with

$$\begin{aligned} H_g \;=\; & \sum_{j=1}^{3}\Omega_1 P_{j-1}^0\sigma_j^{rg}P_{j+1}^0\,\mathrm{e}^{-\mathrm{i}\Delta_1 t} + \sum_{j=1}^{2}\Omega_2 P_{j-1}^0\sigma_j^{rg}P_{j+1}^1 \\ & + \sum_{j=2}^{3}\Omega_2 P_{j-1}^1\sigma_j^{rg}P_{j+1}^0 + \Omega_3 P_1^1\sigma_2^{rg}P_3^1\,\mathrm{e}^{\mathrm{i}\Delta_1 t} \\ & + \Omega_4(P_3^1\sigma_1^{rg}P_2^0 + P_2^0\sigma_3^{rg}P_1^1) \\ & + \Omega_5(P_3^1\sigma_1^{rg}P_2^1 + P_2^1\sigma_3^{rg}P_1^1)\,\mathrm{e}^{\mathrm{i}\Delta_1 t} + \mathrm{H.c.}, \\ H_e \;=\; & \sum_{j=1}^{3}\Omega_0 P_{j-1}^0\sigma_j^{er}P_{j+1}^0 + \mathrm{H.c.}, \end{aligned}$$

where the projection operators are defined as $P_j^0 = |g_j\rangle\langle g_j|$, $P_j^1 = |r_j\rangle\langle r_j|$ with the periodic boundary conditions $P_0 = P_3$ and $P_4 = P_1$. Meanwhile, in order to achieve the desired Rydberg antiblockade regime of $H_g$, we have set $U = \Delta_2 = (\Delta_3 + \Delta_1)/2$, $\Delta_4 = U/8$, $\Delta_1 + \Delta_5 = 9U/8$, and $\Delta_1 = 2\Omega_2$. Note that the other terms, including two or more atoms in state $|e\rangle$, have been disregarded safely because of the large detuning conditions $U \gg \Omega_{0,1,2,3,4,5}$; thus, the corresponding Lindblad operators can be reduced as $L^j = \sqrt{\Gamma}P_{j-1}^0\sigma_j^{ge}P_{j+1}^0$. Furthermore, under the assumption that the spontaneous emission rate $\Gamma$ is much stronger than the coupling strength $\Omega_0$, the level $|e\rangle$ can be adiabatically eliminated and thence leading to an effective Lindblad operator $L_{\mathrm{eff}}^j = \sqrt{4\Omega_0^2/\Gamma}P_{j-1}^0\sigma_j^{gr}P_{j+1}^0$. The corresponding master equation for this case is derived as

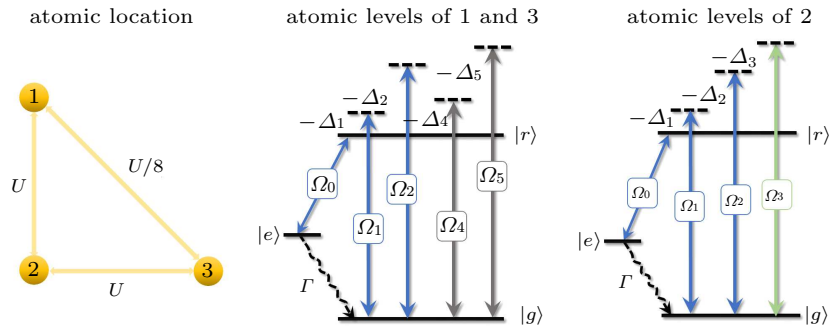



**Fig. 1.** The alignment and energy level structure diagram of three identical Rydberg atoms. $|g\rangle$, $|r\rangle$, and $|e\rangle$ denote the ground state, the Rydberg excited state, and a temporary level, respectively. Here we have set the state $|e\rangle$ spontaneously decays into the ground state with rate $\Gamma$. For atoms 1 and 3, the transitions from $|g\rangle$ to $|r\rangle$ is realized by the polychromatic fields $\Omega_{1,2,4,5}$, and the transition $|g\rangle \leftrightarrow |r\rangle$ of atom 2 is driven by the polychromatic fields $\Omega_{1,2,3}$. In addition, the resonant transition $|e\rangle \leftrightarrow |r\rangle$ of the three Rydberg atoms is coupled to the classical laser of Rabi frequency $\Omega_0$.

$$\dot{\rho} = -\mathrm{i}[H_g,\rho] + \sum_{j=1}^{3}\left[L_{\mathrm{eff}}^{j}\rho L_{\mathrm{eff}}^{j\dagger} - \frac{1}{2}(L_{\mathrm{eff}}^{j\dagger}L_{\mathrm{eff}}^{j}\rho + \rho L_{\mathrm{eff}}^{j\dagger}L_{\mathrm{eff}}^{j})\right]. \quad (4)$$

In order to explore the mechanism of the current scheme more clearly, we rewrite $H_g$ in terms of the basis of $\{|\mathrm{GHZ}_{\pm}\rangle, |\Psi_{1\pm}\rangle, |\Psi_{2\pm}\rangle, |\Psi_{3\pm}\rangle\}$, where $|\Psi_{1\pm}\rangle = (|grr\rangle + |rgr\rangle + |rrg\rangle \pm |ggr\rangle \pm |grg\rangle \pm |rgg\rangle)/\sqrt{6}$, $|\Psi_{2\pm}\rangle = (|rrg\rangle - |grr\rangle \pm |rgg\rangle \mp |ggr\rangle)/2$, and $|\Psi_{3\pm}\rangle = (2|rgr\rangle - |grr\rangle - |rrg\rangle \mp 2|grg\rangle \pm |ggr\rangle \pm |rgg\rangle)/2\sqrt{3}$ are the eigenvectors of the resonant terms of $H_g$, and $|\mathrm{GHZ}_{\pm}\rangle = (|ggg\rangle \pm |rrr\rangle)/\sqrt{2}$. Then the Hamiltonian $H_g$ reduces to

$$\begin{aligned} H_g = {} & \sqrt{3}\Omega(|\mathrm{GHZ}_+\rangle\langle\Psi_{1+}| - |\mathrm{GHZ}_-\rangle\langle\Psi_{1-}|)\mathrm{e}^{\mathrm{i}\Delta_1 t} + \mathrm{H.c.} \\ & + \Omega_2(2|\Psi_{1+}\rangle\langle\Psi_{1+}| - 2|\Psi_{1-}\rangle\langle\Psi_{1-}| + |\Psi_{2+}\rangle\langle\Psi_{2+}| \\ & - |\Psi_{2-}\rangle\langle\Psi_{2-}| + |\Psi_{3+}\rangle\langle\Psi_{3+}| - |\Psi_{3-}\rangle\langle\Psi_{3-}|), \end{aligned} \quad (5)$$

where we have set $\Omega_1 = \Omega_3 = \Omega_5 = \Omega$, $\Omega_4 = \Omega_2$ for simplicity. From Eq. (5), we can find that the present scheme has two transition channels $|\mathrm{GHZ}_{\pm}\rangle \leftrightarrow |\Psi_{\pm}\rangle$ corresponding to detuning $\Delta_1 \mp 2\Omega_2$. Once we choose $\Delta_1 = 2\Omega_2$ and $\Omega_2 \gg \Omega$, it is reasonable to neglect the high-frequency oscillatory terms and only keep the resonant transition $|\mathrm{GHZ}_+\rangle \leftrightarrow |\Psi_{1+}\rangle$. Finally, the total Hamiltonian can be simplified as

$$\begin{aligned} H_{\mathrm{eff}} = {} & \sqrt{3}\Omega|\mathrm{GHZ}_+\rangle\langle\Psi_{1+}| + \mathrm{H.c.} + \Omega_2\big(|\Psi_{2+}\rangle\langle\Psi_{2+}| \\ & - |\Psi_{2-}\rangle\langle\Psi_{2-}| + |\Psi_{3+}\rangle\langle\Psi_{3+}| - |\Psi_{3-}\rangle\langle\Psi_{3-}|\big), \end{aligned} \quad (6)$$

and the corresponding effective master equation of the whole system can be summarized as

$$\dot{\rho} = -\mathrm{i}[H_{\mathrm{eff}},\rho] + \sum_{j=1}^{3}\left[L_{\mathrm{eff}}^{j}\rho L_{\mathrm{eff}}^{j\dagger} - \frac{1}{2}\left(L_{\mathrm{eff}}^{j\dagger}L_{\mathrm{eff}}^{j}\rho + \rho L_{\mathrm{eff}}^{j\dagger}L_{\mathrm{eff}}^{j}\right)\right]. \quad (7)$$

Clearly from Eqs. (6) and (7), we can find that $|\mathrm{GHZ}_-\rangle$ is the unique steady state of the effective system on account of $H_{\mathrm{eff}}(L_{\mathrm{eff}}^{j})|\mathrm{GHZ}_-\rangle = 0$ $(j = 1,2,3)$. Therefore, for an arbitrary initial state, it will be finally converged into the steady state $|\mathrm{GHZ}_-\rangle$ by the processes of pumping and decaying. In Fig. 2, we plot the temporal evolutions of our system from a fully mixed initial state $\rho_0 = \sum_{l,m,n} P_1^l P_2^m P_3^n/8$ $(l,m,n = 0,1)$ with parameters $\Omega_0 = 0.8\Omega_2$, $\Omega_1 = \Omega_3 = \Omega_5 = 0.06\Omega_2$, $\Omega_2 = \Omega_4$, $\Gamma = 6\Omega_2$, and $U = 500\Omega_2$, where the measure of population for state $|\mathrm{GHZ}_{\pm}\rangle$ is defined as $P_{\mathrm{GHZ}_{\pm}} = \langle\mathrm{GHZ}_{\pm}|\rho(t)|\mathrm{GHZ}_{\pm}\rangle$. The solid line and empty circles are simulated by the full master equation Eq. (1) and the effective master equation Eq. (7), respectively. It can be seen that the full and effective dynamics bear an excellent level of consistency, which implies that the effective master equation is exact and it provides a reasonable approximation for us to explain the behavior of the original system. On the other hand, the population of the target state $|\mathrm{GHZ}_-\rangle$ can reach 99.44% within time $200/\Omega_2$, and the population of state $|\mathrm{GHZ}_+\rangle$ nearly disappears (0.3%).

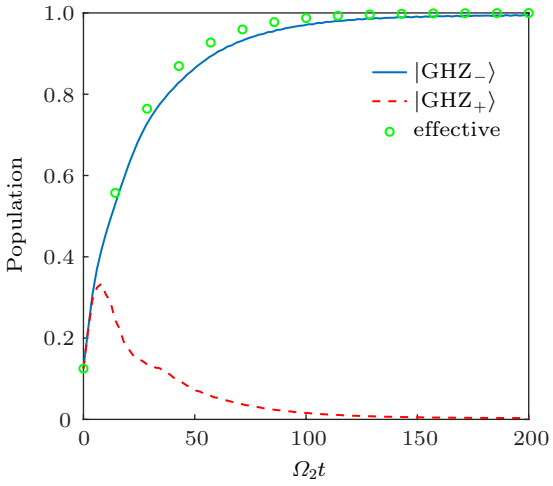



**Fig. 2.** The populations of states $|\mathrm{GHZ}_-\rangle$ (blue solid line) and $|\mathrm{GHZ}_+\rangle$ (red dotted line) are plotted as functions of $\Omega_2 t$ with the initial state $\rho_0 = \sum_{l,m,n} P_1^l P_2^m P_3^n/8$ $(l,m,n = 0,1)$. The green empty circles simulate the dynamics derived from the effective master equation Eq. (7). The parameters are chosen as $\Omega_0 = 0.8\Omega_2$, $\Omega_1 = \Omega_3 = \Omega_5 = 0.06\Omega_2$, $\Omega_2 = \Omega_4$, $\Gamma = 6\Omega_2$, and $U = 500\Omega_2$.

### 2.2. Optimization based on Lyapunov control

Lyapunov control is a sufficiently powerful control technique for quantum control tasks,[76–86] in which the key of the method is to select a series of appropriate Lyapunov functions. By designing the time-varying control fields, one can drive a quantum system to a target state or realize some specific operations. Based on Lyapunov control, we will optimize the above dissipative scheme to speed up the evolution to the target state and release the limiting conditions for the strengths of polychromatic driving fields. The general formula of quantum Lyapunov control to describe the evolution of system reads

$$\dot{\rho} = -\mathrm{i}[H + \sum_{n} f_n(t)H_n,\rho] + \mathcal{L}_{\rho}, \quad (8)$$

with

$$\mathcal{L}_{\rho} = \sum_{j=1}^{3} L_j\rho L_j^{\dagger} - \frac{1}{2}(L_j^{\dagger}L_j\rho + \rho L_j^{\dagger}L_j),$$

where $H_n$ are time-independent Hamiltonian corresponding to different types of external control, and $f_n(t)$ are the time-varying control fields established by Lyapunov function. Notice that the choice of Lyapunov function is not unique. In this paper, we consider the Lyapunov function in the following form:[87]

$$V(t) = \mathrm{Tr}(\rho\rho_t), \quad (9)$$

where $\rho_t$ is the density matrix of the target state $|\mathrm{GHZ}_-\rangle$. Obviously, we can find that $V(t)$ approaches a maximum value $V(t) = 1$ as the system evolves into the target state. It is not hard to calculate that the first-order time derivative of $V(t)$ is

$$\dot{V}(t) = \mathrm{Tr}[(-\mathrm{i}[H,\rho] + \mathcal{L}_{\rho})\rho_t] + \sum_{n} f_n(t)\mathrm{Tr}[(-\mathrm{i}[H_n,\rho])\rho_t]. \quad (10)$$

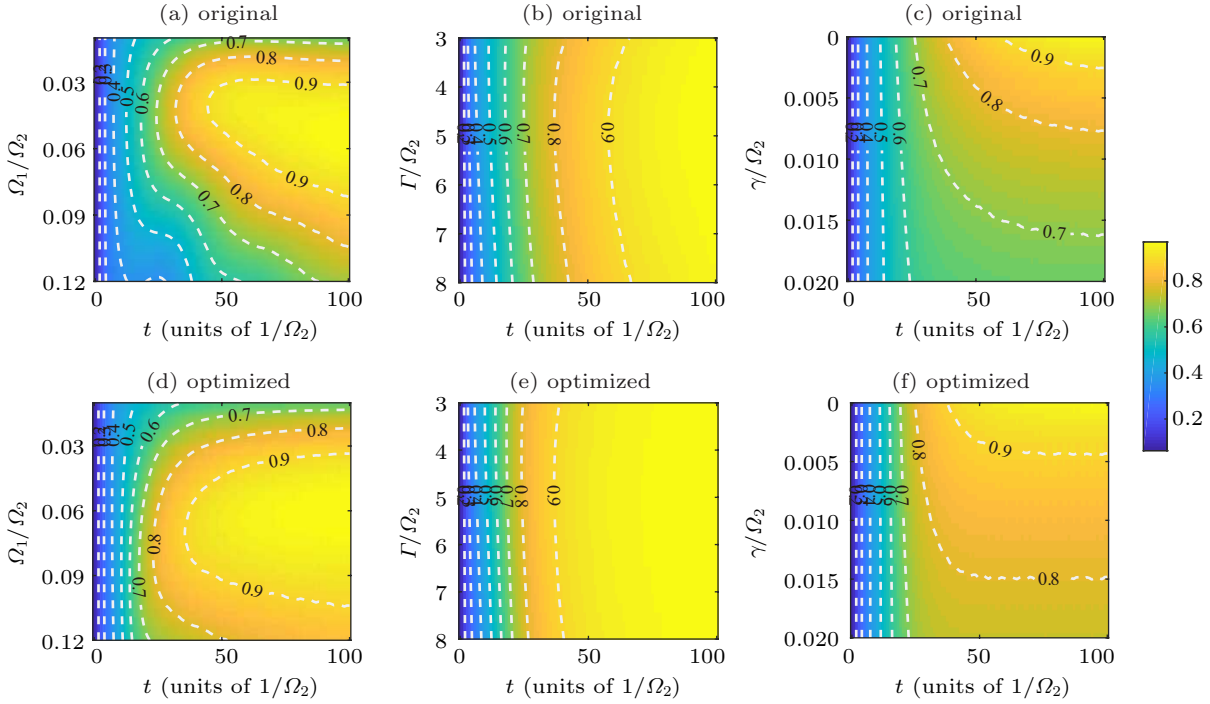



**Fig. 3.** Comparison with respect to the time-dependent population of state $|\mathrm{GHZ}_-\rangle$ between the original scheme and optimized scheme. The populations are governed by Eqs. (1) and (8) containing the decay of Rydberg states, respectively. (a) [(d)] The population for target state versus the coupling strength $\Omega_1/\Omega_2$ with $\gamma = 0$ and $\Gamma = 6\Omega_2$. (b) [(e)] The population for target state versus the decay rate $\Gamma$ of the state $|e\rangle$ with $\gamma = 0$ and $\Omega_1 = 0.06\Omega_2$. (c) [(f)] The population for target state versus the atomic spontaneous emission $\gamma$ of Rydberg state with $\Omega_1 = 0.06\Omega_2$ and $\Gamma = 6\Omega_2$. The other parameters are chosen as $\Omega_0 = 0.8\Omega_2$, $\Omega_3 = \Omega_5 = 0.06\Omega_2$, $\Omega_2 = \Omega_4$, and $U = 500\Omega_2$.

For $V$ to be a Lyapunov function, the control functions $f_n(t)$ should be chosen to satisfy $\dot{V}(t) \geqslant 0$. A simple and conventional way is to let[83]

$$f_n(t) = \mathrm{Tr}\left[(-\mathrm{i}\left[H_n, \rho\right])\rho_t\right]. \tag{11}$$

In order to make the additional coherent control field easy to be achieved and modulated in the experiment, we choose the control Hamiltonians $H_n$ as $H_1 = \mu_1\sigma_1^{rg}\mathrm{e}^{-\mathrm{i}\Delta_1 t} + \mathrm{H.c.}$, $H_2 = \mu_2\sigma_2^{rg}\mathrm{e}^{-\mathrm{i}\Delta_1 t} + \mathrm{H.c.}$, $H_3 = \mu_3\sigma_3^{rg}\mathrm{e}^{-\mathrm{i}\Delta_1 t} + \mathrm{H.c.}$, $H_4 = \mu_4\sigma_1^{rg}\mathrm{e}^{-\mathrm{i}\Delta_5 t} + \mathrm{H.c.}$, $H_5 = \mu_5\sigma_2^{rg}\mathrm{e}^{-\mathrm{i}\Delta_3 t} + \mathrm{H.c.}$, and $H_6 = \mu_6\sigma_3^{rg}\mathrm{e}^{-\mathrm{i}\Delta_5 t} + \mathrm{H.c.}$, where $\mu_j$ are the time-independent parameters used to modulate the intensities of the control fields (the coefficients are chosen as $\mu_1 = \mu_2 = \mu_3 = 0.1\Omega_2$ and $\mu_4 = \mu_5 = \mu_6 = 0.6\Omega_2$). To show the optimized scheme with Lyapunov control in detail, we compare the population of the target state versus the corresponding parameters for the original scheme and the optimized one in Fig. 3. As shown in Fig. (a), to obtain the target state $|\mathrm{GHZ}_-\rangle$ in the population 90% at the evolution time $t = 100/\Omega_2$, the coupling strength $\Omega_1$ should be in the range of $0.032\Omega_2$ to $0.081\Omega_2$. While in Fig. 3(d), it can be seen that the permitted range of $\Omega_1$ has been widened. Even at $\Omega_1 = 0.1\Omega_2$, the population of the target state can still reach 90%. Comparing Fig. 3(b) with Fig. 3(e), it is shown that the speed approaching the target state has been improved. Taking the case of $\Gamma = 6/\Omega_2$ as an example, the evolution time to reach the population 90% of the target state has been shortened from $t = 59/\Omega_2$ to $t = 38/\Omega_2$. In addition, although the original scheme can successfully prepare the target state in the presence of the next-nearest neighbor interaction, the scheme is susceptible to the spontaneous emission of the Rydberg state $|r\rangle$. From Figs. 3(c) and 3(f), we can see that the robustness of the optimized system against the atomic spontaneous emission $\gamma$ has been enhanced. Under the condition $\gamma/\Omega_2 \in (0, 0.015)$ and $t/\Omega_2 \in (30, 100)$, the population of target state was increased from 70% to 80%.

## 3. Generalize to four-partite systems

Now, we extend the proposal for the preparation of the GHZ states to a four-partite system, which consists of four identical Rydberg atoms arranged in a square with sides of length $R$, as shown in Fig. 4. The transitions $|g\rangle \leftrightarrow |r\rangle$ and $|e\rangle \leftrightarrow |r\rangle$ are coupled by two polychromatic fields with detunings $-\Delta_j$ and $-\Delta_j'$ and coupling strengths $\Omega_j$ and $\omega_j$, respectively ($j = 1, 2, 3, 4$). The corresponding full master equation in the absence of Rydberg decay can be written as

$$\dot{\rho} = -\mathrm{i}[H_f, \rho] + \sum_{j=1}^{4} L_j\rho L_j^\dagger - \frac{1}{2}(L_j^\dagger L_j\rho + \rho L_j^\dagger L_j), \tag{12}$$

with

$$H_f = \sum_{j=1}^{4}(\omega_j\sigma_j^{re}\mathrm{e}^{-\mathrm{i}\Delta_j' t} + \Omega_j\sigma_j^{rg}\mathrm{e}^{-\mathrm{i}\Delta_j t} + \mathrm{H.c.}) + \sum_{j\neq k} U_{jk}\sigma_j^{rr}\sigma_k^{rr},$$

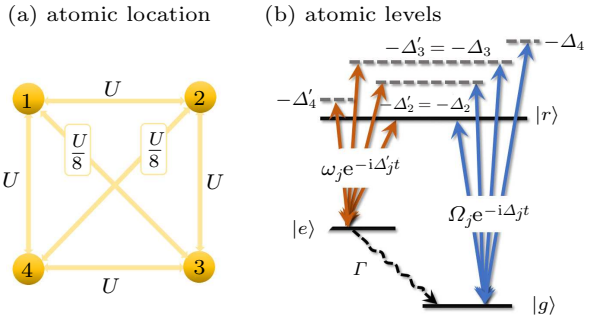



**Fig. 4.** The alignment and energy level structure diagram of four identical Rydberg atoms. $|g\rangle$ , $|r\rangle$, and $|e\rangle$ denote the ground state, the excited Rydberg state, and a short-lived temporary level, respectively.

where $L_j=\sqrt{\Gamma}\sigma_j^{ge}$, and we set the Rydberg interaction $U_{12}=U_{23}=U_{34}=U_{14}=U$ and $U_{13}=U_{24}=U/8$, and the detunings $\Delta_1=\Delta_1'=0$, $\Delta_2=\Delta_2'=U$, $\Delta_3=\Delta_3'=9U/8$, $\Delta_4=17U/8$, and $\Delta_4'=U/8$. Similar to the derivation of Sec. 2, in the large decay condition of $\Gamma\gg\omega_j$, we can adiabatically eliminate the state $|e\rangle$ to obtain the effective Lindblad operators

$$\begin{aligned}
L_{\rm eff}^1&=\sqrt{4\omega_1^2/\Gamma}\sum_{j=1}^4 P_{j-1}^0\sigma_j^{gr}P_{j+1}^0P_{j+2}^0,\\
L_{\rm eff}^2&=\sqrt{4\omega_2^2/\Gamma}\sum_{j=1}^4 P_{j-1}^0\sigma_j^{gr}P_{j+1}^1,\\
L_{\rm eff}^3&=\sqrt{4\omega_3^2/\Gamma}\sum_{j=1}^4 P_{j-1}^1\sigma_j^{gr}P_{j+1}^0,\\
L_{\rm eff}^4&=\sqrt{4\omega_4^2/\Gamma}\sum_{j=1}^4 P_{j-1}^0\sigma_j^{gr}P_{j+1}^0P_{j+2}^1,
\end{aligned}$$

and periodic boundary conditions of $j$ is considered, *i.e.*, $P_0=P_4$ and $P_5=P_1$. In the limiting condition of $U\gg(\Omega_j,\omega_j)$, we can reformulate the Hamiltonian in the following form:

$$\begin{aligned}
H_f=&-\frac{\Omega}{\sqrt{2}}|{\rm GHZ}_-\rangle\Big(\langle\Phi_4|+\frac{1}{\sqrt{2}}\langle\Phi_5|+\langle\Phi_6|+\langle\Phi_7|\Big)\\
&+\Omega|{\rm GHZ}_+\rangle(\langle\Phi_{1+}|+\langle\Phi_{1-}|)+{\rm H.c.}\\
&+2\Omega_2\Big(\sqrt{2}|\Phi_{1+}\rangle\langle\Phi_{1+}|-\sqrt{2}|\Phi_{1-}\rangle\langle\Phi_{1-}|\\
&+|\Phi_{2+}\rangle\langle\Phi_{2+}|-|\Phi_{2-}\rangle\langle\Phi_{2-}|+|\Phi_{3+}\rangle\langle\Phi_{3+}|\\
&-|\Phi_{3-}\rangle\langle\Phi_{3-}|\Big),
\end{aligned}\tag{13}$$

where we have set $\Omega_1=\Omega_4=\Omega$, $\Omega_2=\Omega_3$, and $|{\rm GHZ}_\pm\rangle=(|gggg\rangle\pm|rrrr\rangle)/\sqrt{2}$. When we choose $\Omega_2\gg\Omega$, the effective Hamiltonian can be expressed as

$$\begin{aligned}
H_{\rm eff}^f=&-\frac{\Omega}{\sqrt{2}}|{\rm GHZ}_-\rangle\Big(\langle\Phi_4|+\frac{1}{\sqrt{2}}\langle\Phi_5|+\langle\Phi_6|+\langle\Phi_7|\Big)\\
&+{\rm H.c.}+2\Omega_2\Big(|\Phi_{2+}\rangle\langle\Phi_{2+}|-|\Phi_{2-}\rangle\langle\Phi_{2-}|\\
&+|\Phi_{3+}\rangle\langle\Phi_{3+}|-|\Phi_{3-}\rangle\langle\Phi_{3-}|\Big),
\end{aligned}\tag{14}$$

with

$$\begin{aligned}
|\Phi_{1\pm}\rangle=&\frac{1}{4}(|gggr\rangle+|ggrg\rangle+|grgg\rangle+|rggg\rangle)\\
&\pm\frac{1}{2\sqrt{2}}(|rggr\rangle+|ggrr\rangle+|grrg\rangle+|rrgg\rangle)\\
&+\frac{1}{4}(|grrr\rangle+|rgrr\rangle+|rrgr\rangle+|rrrg\rangle),\\
|\Phi_{2\pm}\rangle=&\frac{1}{2\sqrt{2}}(|grgg\rangle+|rrrg\rangle-|rgrr\rangle-|gggr\rangle)\\
&+\frac{1}{2\sqrt{2}}(\pm|grrg\rangle\pm|rrgg\rangle\mp|rggr\rangle\mp|ggrr\rangle),\\
|\Phi_{3\pm}\rangle=&\frac{1}{2\sqrt{2}}(|rggg\rangle+|rrgr\rangle-|grrr\rangle-|ggrg\rangle)\\
&+\frac{1}{2\sqrt{2}}(\pm|rggr\rangle\pm|rrgg\rangle\mp|ggrr\rangle\mp|grrg\rangle),\\
|\Phi_4\rangle=&\frac{1}{2\sqrt{2}}(|rrrg\rangle-|grgg\rangle),\\
|\Phi_5\rangle=&\frac{1}{2}(|ggrg\rangle+|rrgr\rangle-|gggr\rangle-|grgg\rangle),\\
|\Phi_6\rangle=&\frac{1}{\sqrt{2}}(|rgrr\rangle-|gggr\rangle),\\
|\Phi_7\rangle=&\frac{1}{\sqrt{2}}(|grrr\rangle-|ggrg\rangle).
\end{aligned}$$

Then the corresponding effective master equation takes the following form

$$\dot\rho=-{\rm i}[H_{\rm eff},\rho]+\sum_{j=1}^4\Big[L_{\rm eff}^j\rho L_{\rm eff}^{j\dagger}-\frac{1}{2}(L_{\rm eff}^{j\dagger}L_{\rm eff}^j\rho+\rho L_{\rm eff}^{j\dagger}L_{\rm eff}^j)\Big].\tag{15}$$

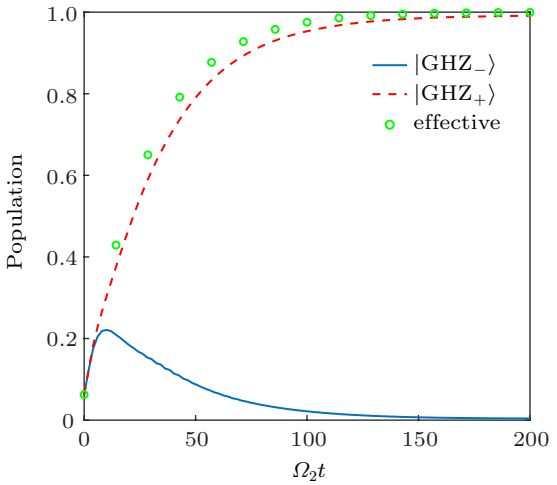



**Fig. 5.** The populations of states $|{\rm GHZ}_-\rangle$ (blue solid line) and $|{\rm GHZ}_+\rangle$ (red dotted line) are plotted as functions of $\Omega_2 t$ with the initial state $\rho_0=\sum_{l,m,n}P_1^kP_2^lP_3^mP_4^n/16$ $(k,l,m,n=0,1)$. The green empty circles simulate the dynamics derived from the effective master equation Eq. (15). The parameters are chosen as $\omega_1=0.8\Omega_2$, $\omega_2=\omega_3=\omega_4=0.24\Omega_2$, $\Omega_1=\Omega_4=0.05\Omega_2$, $\Omega_2=\Omega_3$, $\Gamma=6\Omega_2$, and $U=300\Omega_2$.

In Fig. 5, we numerically simulate the evolution of the populations for states $|{\rm GHZ}_+\rangle$, $|{\rm GHZ}_-\rangle$ governed by the full master equation Eq. (12) and the effective master equation Eq. (15). We find that the system ultimately evolves into the target state $|{\rm GHZ}_+\rangle$. Moreover, the population of $|{\rm GHZ}_+\rangle$ (empty circle) governed by the effective master equation Eq. (15) is in great agreement with the solid line. Similar to the method in the last section, we further use Lyapunov control to optimize the scheme for preparing the GHZ state of the four-partite system. The additional coherent control fields can be chosen as $H_1=\lambda_1\sigma_1^{rg}+{\rm H.c.}$, $H_2=\lambda_2\sigma_2^{rg}+{\rm H.c.}$, $H_3=\lambda_3\sigma_3^{rg}+{\rm H.c.}$, $H_4=\lambda_4\sigma_4^{rg}+{\rm H.c.}$, $H_5=\lambda_5\sigma_1^{rg}e^{-i\Delta_4 t}+{\rm H.c.}$, $H_6=\lambda_6\sigma_2^{rg}e^{-i\Delta_4 t}+{\rm H.c.}$, $H_7=\lambda_7\sigma_3^{rg}e^{-i\Delta_4 t}+{\rm H.c.}$, and $H_8=\lambda_8\sigma_4^{rg}e^{-i\Delta_4 t}+{\rm H.c.}$ Then, we can get the optimized mas-

ter equation of this four-partite system

$$\dot{\rho} = -\mathrm{i}\left[H_f + \sum_n f_n(t)H_n, \rho\right] + \sum_{j=1}^{4} L_j \rho L_j^{\dagger} - \frac{1}{2}(L_j^{\dagger}L_j\rho + \rho L_j^{\dagger}L_j). \quad (16)$$

In order to investigate the optimization effect of Lyapunov control on this system, we plot the comparison diagram of the time-dependent population for target state $|\mathrm{GHZ}_+\rangle$ versus the decay rate $\Gamma$, coupling strength $\Omega_1$, and atomic spontaneous emission $\gamma$ governed by Eqs. (12) and (16) in Fig. 6, the coefficients $\lambda_j$ are set as $\lambda_1 = \lambda_2 = \lambda_3 = \lambda_4 = 0.1\Omega_2$, $\lambda_5 = \lambda_6 = \lambda_7 = \lambda_8 = 0.8\Omega_2$, and the other parameters are consistent with those of Fig. 5. Although the degree of acceleration is not as good as that of the three-partite system, the release of the constraint conditions and the robustness against the spontaneous emissions of Rydberg states are significantly enhanced.

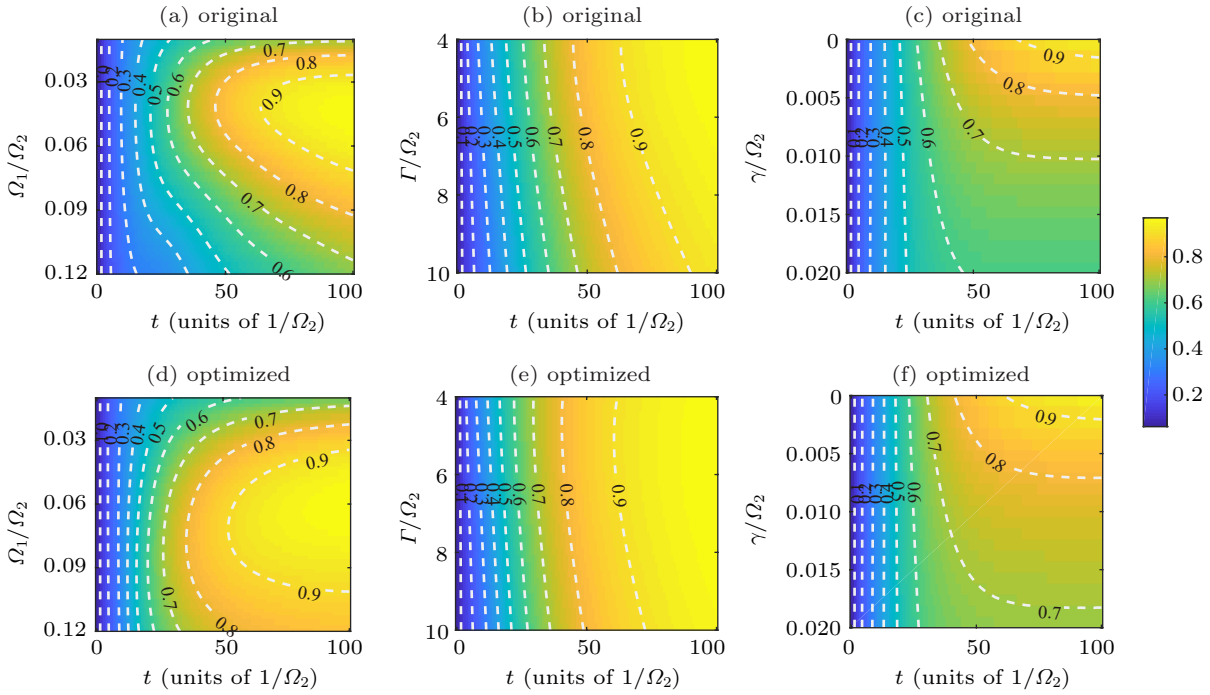



**Fig. 6.** Comparison with respect to the time-dependent population of state $|\mathrm{GHZ}_+\rangle$ between the original scheme and optimized scheme. The populations are simulated on the basis of Eqs. (12) and (16) by considering the spontaneous emissions of Rydberg states, respectively. (a) [(d)] The population for target state versus the coupling strength $\Omega_1/\Omega_2$ with $\gamma = 0$ and $\Gamma = 6\Omega_2$. (b) [(e)] The population for target state versus the decay rate $\Gamma$ of the state $|e\rangle$ with $\gamma = 0$ and $\Omega_1 = 0.05\Omega_2$. (c) [(f)] The population for target state versus the atomic spontaneous emission $\gamma$ of Rydberg state with $\Omega_1 = 0.05\Omega_2$ and $\Gamma = 6\Omega_2$. The other parameters are chosen as $\omega_1 = 0.8\Omega_2$, $\omega_2 = \omega_3 = \omega_4 = 0.24\Omega_2$, $\Omega_2 = \Omega_3$, $\Omega_4 = 0.05\Omega_2$ and $U = 300\Omega_2$.

## 4. Experimental feasibility

Finally, we give some discussion on the experimental feasibility of our scheme. Our model is composed of Rydberg atoms arranged in different geometric shapes, which is a feasible technique in many experiments.[88–90] In Ref. [89], Nogrette *et al.* trap single $^{87}$Rb atoms in the sites of arrays containing up to approximately 100 microtraps separated by distances as small as 3 μm, with geometries ranging from simple square or triangular lattices to more complex ones, such as kagome or honeycomb structures. Here we may employ $^{87}$Rb with Rydberg state $|r\rangle \equiv |80\mathrm{S}_{1/2}\rangle$, and the corresponding Rydberg-Rydberg interaction is $U_{rr} = C_6/r^6$, where $C_6 = 2\pi \times 4162.712$ GHz·μm$^6$.[75,91] We set the atomic distances in the three-particle system and four-particle system as $r = 4.502$ μm and $r = 4.902$ μm, and the corresponding strengths $U$ are $2\pi \times 500$ MHz and $2\pi \times 300$ MHz, respectively.

In a realistic Rydberg-atom system, we also need to consider the atomic spontaneous emissions of Rydberg states. Beterov *et al.*[92] provided the results of the calculations of effective lifetimes of Rydberg states and compared them with available experimental and theoretical data. According to the analytical formula for estimating the effective lifetime $\tau_0 = \tau_s n_{\mathrm{eff}}^{\delta}$ at $T = 0$ K, we can calculate the decay rate of Rydberg state $|r\rangle \equiv |80\mathrm{S}_{1/2}\rangle$ is $\gamma = 2\pi \times 0.255$ kHz. And the decay rate of the temporary state can be chosen as $\Gamma = 2\pi \times 6.1$ MHz and the strength of the driving fields $\Omega_2 = 2\pi \times 1$ MHz.[93] In Fig. 7, we perform the numerical simulation with the above parameters based on the definition of the fidelity $F = \mathrm{Tr}\left[\rho_{\mathrm{GHZ}_\pm}^{1/2}\rho(t)\rho_{\mathrm{GHZ}_\pm}^{1/2}\right]^{1/2}$. The experimental feasibilities of the three- and four-partite systems are adequately exhibited by the fidelity of up to 99.24% and 98.76%, respectively, which are relatively high in the sense of multipartite steady-state entanglement.

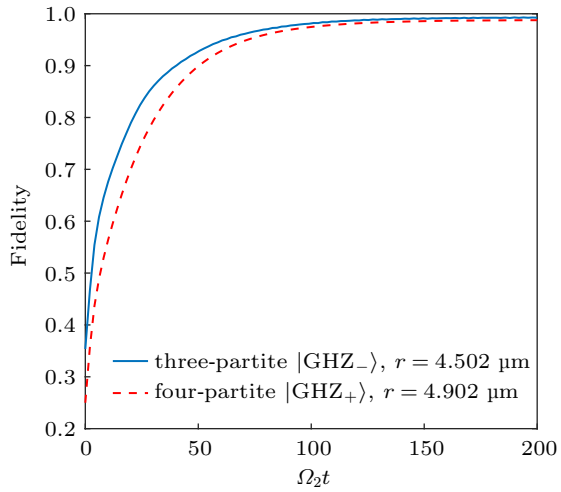



**Fig. 7.** The fidelity of target state diagram simulated according to experimental parameters. The solid blue line and the dotted red line indicate the three- and four-particle system of optimized schemes, respectively. The initial states and other parameters of the three- and four-partite system in the numerical simulation are consistent with those in Figs. 2 and 5, respectively.

## 5. Summary

In summary, we have systematically investigated the feasibility of preparing GHZ states in three- and four-partite systems by using Rydberg antiblockade and the engineered spontaneous emissions of Rydberg states in the presence of the next-nearest neighbor interaction of Rydberg atoms. The introduction of additional control fields according to Lyapunov control enables us to accelerate the dynamic evolution of the system, release the original constraints for the polychromatic driving fields, and enhance the robustness against the spontaneous decay of the excited Rydberg state. We hope that our work may provide a new prospect with regard to the dissipation-based quantum information processing of neutral atoms.

## References


[1] Briegel H J, Dür W, Cirac J I and Zoller P 1998 *Phys. Rev. Lett.* **81** 5932
[2] Bennett C H and DiVincenzo D P 2000 *Nature* **404** 247
[3] Deng F G, Long G L and Liu X S 2003 *Phys. Rev. A* **68** 042317
[4] Deng F G and Long G L 2004 *Phys. Rev. A* **69** 052319
[5] Gisin N and Thew R 2007 *Nat. Photon.* **1** 165
[6] Sheng Y B, Deng F G and Long G L 2010 *Phys. Rev. A* **82** 032318
[7] Andrew S 1998 *Rep. Prog. Phys.* **61** 117
[8] Raussendorf R and Briegel H J 2001 *Phys. Rev. Lett.* **86** 5188
[9] Ladd T D, Jelezko F, Laflamme R, Nakamura Y, Monroe C and OBrien J L 2010 *Nature* **464** 45
[10] Buluta I, Ashhab S and Nori F 2011 *Rep. Prog. Phys.* **74** 104401
[11] Fei S M 2020 *Quantum Engineering* **2** e48
[12] Yang L, Ma H Y, Zheng C, Ding X L, Gao J C and L G L 2017 *Acta Phys. Sin.* **66** 230303 (in Chinese)
[13] Braunstein S and van Loock P 2005 *Rev. Mod. Phys.* **77** 513
[14] Wendin G 2017 *Rep. Prog. Phys.* **80** 106001
[15] Flamini F, Spagnolo N and Sciarrino F 2018 *Rep. Prog. Phys.* **82** 016001
[16] Hu X M, Zhang C, Zhang C J, Liu B H, Huang Y F, Han Y J, Li C F and Guo G C 2019 *Quantum Engineering* **1** e13
[17] Jin R B, Cai W H, Ding C, Mei F, Deng G W, Shimizu R and Zhou Q 2020 *Quantum Engineering* **2** e38
[18] Huang W J, Chien W C, Cho C H, Huang C C, Huang T W and Chang C R 2020 *Quantum Engineering* **2** e45
[19] Mastriani M and Iyengar S S 2020 *Quantum Engineering* **2** e55
[20] Yang L, Liu Y C and Li Y S 2020 *Chin. Phys. B* **29** 060301
[21] Liu Y H, Wu L, Yan Z H, Jia X J and Peng K C 2019 *Acta Phys. Sin.* **68** 034202 (in Chinese)
[22] Yang C, Li D X and Shao X Q 2019 *Sci. China-Phys. Mech. & Astron.* **62** 110312
[23] Alioscia H, Radu I and Paolo Z 2005 *Phys. Rev. A* **71** 022315
[24] Gühne O and Toth G 2009 *Phys. Rep.* **474** 1
[25] Ryszard H, Horodecki P, Horodecki M and Horodecki K 2009 *Rev. Mod. Phys.* **81** 865
[26] Pan J W, Chen Z B, Lu C Y, Weinfurter H, Zeilinger A and Żukowski M 2012 *Rev. Mod. Phys.* **84** 777
[27] Hillery M, Bužek V and Berthiaume A 1999 *Phys. Rev. A* **59** 1829
[28] Tittel W, Zbinden H and Gisin N 2001 *Phys. Rev. A* **63** 042301
[29] Chen Y A, Zhang A N, Zhao Z, Zhou X Q, Lu C Y, Peng C Z, Yang T and Pan J W 2005 *Phys. Rev. Lett.* **95** 200502
[30] Karlsson A and Bourennane M 1998 *Phys. Rev. A* **58** 4394
[31] Jin L H, Jin X R and Zhang S 2005 *Phys. Rev. A* **72** 024305
[32] Jung E, Hwang M R, Ju Y H, Kim M S, Yoo S K, Kim H, Park D, Son J W, Tamaryan S and Cha S K 2008 *Phys. Rev. A* **78** 012312
[33] Lee S W, Paternostro M, Lee J and Jeong H 2013 *Phys. Rev. A* **87** 022123
[34] Zhang C, Huang Y F, Wang Z, Liu B H, Li C F and Guo G C 2015 *Phys. Rev. Lett.* **115** 260402
[35] Jiao Y C, Han X X, Yang Z W, Zhao J M and Jia S T 2016 *Chin. Phys. Lett.* **33** 123201
[36] Yan D, Wang B B, Bai W J, Liu B, Du X G and Ren C N 2019 *Acta Phys. Sin.* **68** 084203 (in Chinese)
[37] Li X K, Jia F D, Yu F C, Li M Y, Xue P, Xu X Y and Zhong Z P 2019 *Acta Phys. Sin.* **68** 043201 (in Chinese)
[38] Zhang H X, Fan C H, Cui C L and Wu J H 2020 *Chin. Phys. B* **29** 013204
[39] He S, Liu D, Li M H 2019 *Chin. Phys. B* **28** 080303
[40] Ma D D, Zhang K Y and Qian J 2019 *Chin. Phys. B* **28** 013202
[41] Su S L 2018 *Chin. Phys. B* **27** 110304
[42] Jaksch D, Cirac J I, Zoller, Rolston S L, Côté R and Lukin M D 2000 *Phys. Rev. Lett.* **85** 2208
[43] Weimer H, Muüller M, Lesanovsky I, Zoller P and Büchler H P 2010 *Nat. Phy.* **6** 382
[44] Mølmer K, Isenhower L and Saffman M 2011 *J. Phys. B: A. Mo. Opt. Phys.* **44** 184016
[45] Saffman M and Mølmer K 2009 *Phys. Rev. Lett.* **102** 240502
[46] Zhang X L, Isenhower L, Gill A T, Walker T G and Saffman M 2010 *Phys. Rev. A* **82** 030306
[47] Wilk T, Gaëtan A, Evellin C, Wolters J, Miroshnychenko Y, Grangier P and Browaeys A 2010 *Phys. Rev. Lett.* **104** 010502
[48] Shao X Q, Wu J H and Yi X X 2017 *Phys. Rev. A* **95** 022317
[49] Brion E, Pedersen L, Saffman M and Mølmer K 2008 *Phys. Rev. Lett.* **100** 110506
[50] Han Y and He B, Heshami K, Li C Z, Simon C 2010 *Phys. Rev. A* **81** 052311
[51] Zhao B, Müller M, Hammerer K and Zoller P 2010 *Phys. Rev. A* **81** 052329
[52] Tiarks D, Baur S, Schneider K, Dürr S and Rempe G 2014 *Phys. Rev. Lett.* **113** 053602
[53] Su S L, Guo F Q, Wu J L, Jin Z, Shao X Q and Zhang S 2020 *Europhys. Lett.* **131** 53001
[54] Su S L, Shen H Z, Liang E and Zhang S 2018 *Phys. Rev. A* **98** 032306
[55] Su S L, Guo F Q, Tian L, Zhu X Y, Yan L L, Liang E J and Feng M 2020 *Phys. Rev. A* **101** 012347
[56] Su S L, Liang E J, Zhang S, Wen J J, Sun L L, Jin Z and Zhu A D 2016 *Phys. Rev. A* **93** 042328
[57] Su S L, Tian Y Z, Shen H Z, Zang H P, Liang E J and Zhang S 2017 *Phys. Rev. A* **96** 042335
[58] Zhu X Y, Liang E J and Su S L 2019 *Opt. Soc. Am. B* **36** 1937
[59] Wu J L, Song J and Su S L 2020 *Phys. Lett. A* **384** 126039
[60] Wu J L, Su S L, Wang Y, Song J, Xia Y and Jiang Y Y 2020 *Opt. Lett.* **45** 1200
[61] Su S L, Gao Y, Liang E J and Zhang S 2017 *Phys. Rev. A* **95** 022319
[62] Shao X Q 2020 *Phys. Rev. A* **102** 053118
[63] Tan X, Wu J L, Deng C, Mao W J, Wang H T and Ji X 2018 *Chin. Phys. B* **27** 100307

[64] Carr A W and Saffman M 2013 *Phys. Rev. Lett.* **111** 033607
[65] Shao X Q, Wu J H, Yi X X and Long G L 2017 *Phys. Rev. A* **96** 062315
[66] Shao X Q, You J B, Zheng T Y, Oh C H and Zhang S 2014 *Phys. Rev. A* **89** 052313
[67] Li D X, Shao X Q, Wu J H and Yi X X 2018 *Opt. Lett.* **43** 1639
[68] Li D X, Shao X Q, Wu J H, Yi X X and Zheng T Y 2018 *Opt. Express* **26** 2292
[69] Li R, Yu D M, Su S L and Qian J 2020 *Phys. Rev. A* **101** 042328
[70] Li D X and Shao X Q 2019 *Phys. Rev. A* **99** 032348
[71] Shao X Q, Li D X, Ji Y Q, Wu J H and Yi X X 2017 *Phys. Rev. A* **96** 012328
[72] Shao X Q, Wu J H and Yi X X 2017 *Phys. Rev. A* **95** 062339
[73] Wintermantel T M, Wang Y, Lochead G, Shevate S, Brennen G K and Whitlock S 2020 *Phys. Rev. Lett.* **124** 070503
[74] Li D X, Xiao H W, Yang C, Shao X Q 2020 arXiv: 2004.11570v1 [quant-ph]
[75] Weber S, Tresp C, Menke H, Urvoy A, Firstenberg O, Büchler H P and Hofferberth S 2017 *J. Phys. B: At. Mol. Opt. Phys.* **50** 133001
[76] Cui W and Nori F 2013 *Phys. Rev. A* **88** 063823
[77] Li W L, Li C and Song H S 2016 *Phys. Rev. E* **93** 062221
[78] Hu J, Ke Q and Ji Y H 2016 *Int. J. Mod. Phys. B* **30** 1650177
[79] Leib M and Hartmann M J 2014 *Phys. Rev. Lett.* **112** 223603
[80] Coron J M, Grigoriu A, Lefter C and Turinici G 2009 *New J. Phys.* **11** 105034
[81] Wang X T and Schirmer S G 2009 *Phys. Rev. A* **80** 042305
[82] Hou S C, Khan M A, Yi X X, Dong D Y and Petersen I R 2012 *Phys. Rev. A* **86** 022321
[83] Yi X X, Huang X L, Wu C F and Oh C H 2009 *Phys. Rev. A* **80** 052316
[84] Mazyar M, Pierre R and Gabriel T 2005 *Automatica* **41** 1987
[85] Altafini C 2007 *IEEE Trans. Autom. Control* **52** 2019
[86] Sugawara M 2003 *J. Chem. Phys.* **118** 6784
[87] D'Alessandro D 2007 *Introduction to Quantum Control and Dynamics* (Boca Raton, FL: CRC Press)
[88] Schönleber D W, Eisfeld A, Genkin M, Whitlock S and Wüster S 2015 *Phys. Rev. Lett.* **114** 123005
[89] Nogrette F, Labuhn H, Ravets S, Barredo D, Béguin L, Vernier A, Lahaye T and Browaeys A 2014 *Phys. Rev. X* **4** 021034
[90] Endres M, Bernien H, Keesling A, Levine H, Anschuetz E R, Krajenbrink A, Senko C, Vuletic V, Greiner M and Lukin M D 2018 *New J. Phys.* **20** 013011
[91] Singer K, Stanojevic J, Weidemller M and Robin Côté R 2005 *J. Phys. B: At. Mol. Opt. Phys.* **38** S295
[92] Beterov I I, Ryabtsev I I, Tretyakov D B and Entin V M 2009 *Phys. Rev. A* **79** 052504
[93] Whitlock S, Wildhagen H, Weimer H and Weidemüller M 2019 *Phys. Rev. Lett.* **123** 213606